Journal of Computational Physics **175,** 1–23 (2002)
doi:10.1006/jcph.2001.6855, available online at http://www.idealibrary.com on IDEAL®

A Mixed-Basis Spectral Projection Method

F. Auteri and N. Parolini

Dipartimento di Ingegneria Aerospaziale, Politecnico di Milano, Via La Masa 34, 20158 Milano, Italy
E-mail: auteri@aero.polimi.it

Received September 26, 2000; revised May 23, 2001

A new grid-less (no collocation) spectral projection method is presented. The unsteady Navier–Stokes equations are approximated according to the variational framework of Guermond and Quartapelle which accommodates two vector spaces for the velocity fields obtained in the two half-steps of the fractional-step method but retains only one in the final solution algorithm. Two different bases built on Legendre polynomials are used for the velocity and pressure to solve the corresponding Helmholtz and Poisson equations by direct spectral elliptic solvers. Interpolations $\mathbb{P}_N$ and $\mathbb{P}_{N-2}$ are employed for velocity and pressure to satisfy the LBB stability requirement and a Gauss–Legendre quadrature formula with $\frac{3}{2}N$ integration points is used to prevent aliasing error in the pseudospectral evaluation of the nonlinear terms. A BDF second-order time stepping is implemented to provide accurate numerical results about the stability of the singular driven cavity problem.

Key Words: Navier–Stokes equations; projection method; Galerkin–Legendre spectral methods.

1. INTRODUCTION

The first spectral version of the fractional-step method to solve the incompressible Navier–Stokes equations in the presence of rigid walls was proposed by Gottlieb and Orszag [17] nearly one decade after the projection method was introduced by Chorin [14, 15] and Temam [38] in a finite difference context. In this spectral implementation by the *tau* method, the projection step was performed through a Poisson equation for the pressure before executing the advection–diffusion step, with the nonlinear term evaluated explicitly. Noticeably, the inviscid character of the projection step was taken into account by imposing a boundary condition in this step only on the normal component of velocity [17, p. 146 and 147]. This is in full accordance with Ladyzhenskaya's decomposition theorem which underlies the projection method and confers an essentially different character to the normal boundary condition with respect to the tangential one(s); see also [37].

0021-9991/02 $35.00

The spectral projection method was further elaborated upon by Orszag and Kells, who introduced the idea of a three-step scheme for 3D channel flow simulations [31]. In this method, a purely convective step is performed first. Then, the obtained intermediate velocity is projected onto a divergence-free space and finally a vector parabolic problem is solved, enforcing the complete velocity boundary conditions for the viscous equation. The first two steps are claimed to be second-order accurate in time while the last one is only first-order accurate. This method was employed successfully to simulate the transition to turbulence in Poiseuille and Couette flows between parallel planes. The spectral projection method was later extended to incompressible flows with a variable viscosity by Zang and Hussaini [40]; see also [13, p. 222].

In subsequent studies, the Chorin–Temam projection method was implemented by Ku, Taylor, and Hirsh according to a Chebyshev–collocation approach to compute steady solutions in closed rectangular domains in two [27] and three [28] dimensions. A distinctive feature of their method is the expression of the projection step in the form of a Darcy problem, that is a *grad-div* coupled system for the pressure and velocity unknowns. The discrete counterpart of the continuity equation is satisfied inside the domain as well as on the boundary, in the sense of an assumed collocation scheme. In the words of the authors, satisfying the continuity equation on the boundary provides the lacking boundary condition for the pressure in the projection step. Apparently, the complete no-slip conditions are enforced on either the intermediate or the end-of-step velocity but not on both. In this respect, such a procedure matches properly the aforementioned inviscid character of the projection step and produces accurate two- and three-dimensional results. Also based on a *grad-div* approach and on a Chebyshev–collocation spatial discretization is the splitting technique proposed more recently by Heinrichs [23]. In this case, the Uzawa algorithm is employed in the inviscid step, leading to a pseudo-Laplace equation for the pressure. This splitting has been successfully extended to reach a third-order time accuracy by employing a suitable pressure extrapolation in the first step [24, 25]. Heinrichs' method has been also elaborated upon by Botella [10] who proposed a third-order projection scheme employing Chebyshev polynomials and Gauss–Lobatto collocation, with the incompressible step still expressed in the form of a Darcy problem.

A mathematically more satisfactory treatment of spectral projection methods has been achieved by resorting to the Galerkin variational formulation of the problem of the form well established in the context of finite element approximations many years ago; see e.g. Temam's monograph [37]. Suitable spectral representations based on Legendre polynomials have been introduced by Jie Shen to solve elliptic problems [34] and have been used subsequently to build a Galerkin formulation of the projection method [35]. A second-order version of this method for flows in closed cylindrical geometries has been proposed by Lopez and Shen [30]. This method features a second-order BDF time stepping and is based on the incremental scheme originally formulated by Goda [16] and Van Kan [39], where, differently from Chorin–Temam original scheme, an explicit pressure gradient term appears in the momentum equation. We notice that all the aforementioned higher-order projection schemes make no distinction between the functional spaces in which the intermediate and end-of-step velocities are to be represented.

The fractional-step idea has been pursued also to solve the unsteady version of the Stokes problem with an increasing order of accuracy in time; see for instance the works by Batoul *et al.* and by Karniadakis *et al.* [8, 26]. These spectral methods are however characterized by a coupling between the viscous and incompressible steps through the boundary condition

for pressure, and therefore they can hardly be put under the banner of the class of projection methods.

Many different versions of projection methods have been proposed over the years, but a rigorous analysis about their approximation and stability properties, encompassing both the incremental and non incremental fractional stepping, has been established only recently [33, 35]. In particular, fully discrete projection methods for finite element spatial approximations have been thoroughly investigated by Guermond and Quartapelle [18, 20, 21]. This analysis has pointed out that the structural difference existing between the equations of the two (half) steps requires the introduction of two different functional spaces for the intermediate and end-of-step velocities which are endowed with different regularities, namely $\boldsymbol{H}^1$ and $\boldsymbol{H}^{\mathrm{div}}$, respectively. Indeed, for instance, the normal component of the end-of-step velocity is discontinuous at the element interfaces when standard Lagrangian elements are used. This fact does not entail any difficulty insofar as the same analysis demonstrates that only the intermediate velocity is present in the final solution algorithm, leading to a computer code of the utmost simplicity. These ideas have been further exploited recently by Guermond in a new second-order accurate finite element projection scheme, based on a BDF time discretization for which unconditional stability is obtained through a semi-implicit treatment of the nonlinear term [19].

In this paper we implement the incremental projection method of Guermond and Quartapelle [18, 19, 20, 21] using the second-order BDF time stepping and we introduce an original mixed spectral representation of the Navier–Stokes equations by means of Legendre polynomials. The proposed scheme is similar to the projection method of Lopez and Shen [30] based on Galerkin–Legendre (–Chebyshev) representation and second-order BDF scheme. However, our scheme closely follows Guermond's ideas and analysis, namely, the elimination of the end-of-step velocity, thus getting rid of the low regularity of the $\boldsymbol{H}^{\mathrm{div}}$ space to which such a velocity field belongs. This elimination entails consequences also in the spectral case where the approximate velocity belongs to the space $\mathbb{P}_N \subset C^\infty$, so that the difference of the two velocity spaces must be taken into account to avoid encountering mathematical difficulties [18]. Another element of distinction of the proposed method is that two different polynomial bases are employed to represent the velocity and pressure fields in order to permit the separation of variables in the numerical solution of both the Dirichlet and Neumann boundary value problems for velocity and pressure.

By employing the Galerkin–Legendre spatial discretization and separation of variables proposed in [34], and thanks to the simplicity of the considered projection method, we are able to construct an algorithm that is required to solve, at each time step, Helmholtz and Poisson equations by means of double-diagonalization direct solvers [3]. Characteristic properties of the method are the absence of any grid in the approximation of the linear problem, with all of the discrete spatial operators being evaluated exactly and most of them in closed form, and the banded structure assumed by most of such operators which allows efficient matrix multiplication in the solution algorithm. As far as the nonlinear terms are concerned, the pseudospectral technique is adopted with the aid of the primitive Gauss–Legendre quadrature points. The noncollocative character of the proposed method has two implications: (i) the LBB condition can be satisfied quite naturally by selecting two different polynomial orders for velocity and pressure, thus preventing the occurrence of spurious pressure modes; (ii) aliasing errors in the nonlinear term are avoided by resorting to a quadrature formula of an appropriate order, such as the well-known $\frac{3}{2}N$ rule. By the way,

it is useful to note that the method extends immediately to three dimensions by employing the 3D fast spectral Dirichlet solver given in [4] and the corresponding algorithm for the Neumann problem.

The paper is organized as follows. In Section 2, the mathematical problem is stated in strong form and, after introducing the Legendre spatial approximations, a semi-discrete variational counterpart of the problem is derived. In Section 3, the second-order BDF incremental projection method is presented and the corresponding fully discrete weak problem is given. Section 4 details the various matrices representing the one-dimensional spatial differential operators according to the mixed basis Galerkin–Legendre formulation proposed in the work. Moreover, the Gauss–Legendre-based pseudospectral treatment of the nonlinear terms is described. In Section 5, some numerical tests are presented to verify the predicted error estimates and to assess the efficiency properties of the spectral solver against a stability investigation of the singular driven cavity problem. Finally, Section 6 is devoted to the concluding remarks.

2. FORMULATION OF THE PROBLEM

2.1. The Navier–Stokes Equations

We consider the time-dependent incompressible Navier–Stokes equations formulated in terms of velocity u and pressure p. The complete mathematical statement of the problem is: Find u and p (up to a constant) so that

$$\begin{cases} \dfrac{\partial \boldsymbol{u}}{\partial t} - \nu \nabla^2 \boldsymbol{u} + (\boldsymbol{u} \cdot \boldsymbol{\nabla}) \boldsymbol{u} + \boldsymbol{\nabla} p = \boldsymbol{f}, \\ \boldsymbol{\nabla} \cdot \boldsymbol{u} = 0, \\ \boldsymbol{u}_{|\partial\Omega} = 0, \\ \boldsymbol{u}_{|t=0} = \boldsymbol{u}_0, \end{cases} \tag{2.1}$$

where ν is the viscosity, $\boldsymbol{f}$ is a known body force, and $\boldsymbol{u}_0$ is the divergence-free initial velocity field. For simplicity, we assume homogeneous boundary conditions. The fluid domain Ω is assumed to be the open square $(-1, +1)^2$. The data are assumed to be regular enough and to satisfy all the compatibility conditions needed for a smooth solution to exist for all time; cf., e.g., [32].

2.2. Legendre Spectral Approximation

To build a spectral approximation of problem (2.1) we introduce the finite dimensional space $\boldsymbol{X}_N = (\mathbb{P}_N \otimes \mathbb{P}_N)^2$. We shall approximate the velocity in $\boldsymbol{X}_{0,N} = \boldsymbol{X}_N \cap \boldsymbol{H}_0^1(\Omega)$, and the pressure in $M_{\hat{N}} = \mathbb{P}_{\hat{N}} \otimes \mathbb{P}_{\hat{N}}$, the pressure field being understood to be defined up to an additive constant. The polynomial order N for the velocity is in general different from the polynomial order $\hat{N}$ for the pressure. Here $\boldsymbol{H}_0^1(\Omega)$ is the standard notation for the Sobolev space of vector-valued functions square integrable and with square integrable first derivatives on Ω and with zero trace on $\partial\Omega$.

To recast (2.1) in a weak form by the Galerkin–Legendre spectral method, we consider two different bases for approximating velocity and pressure.

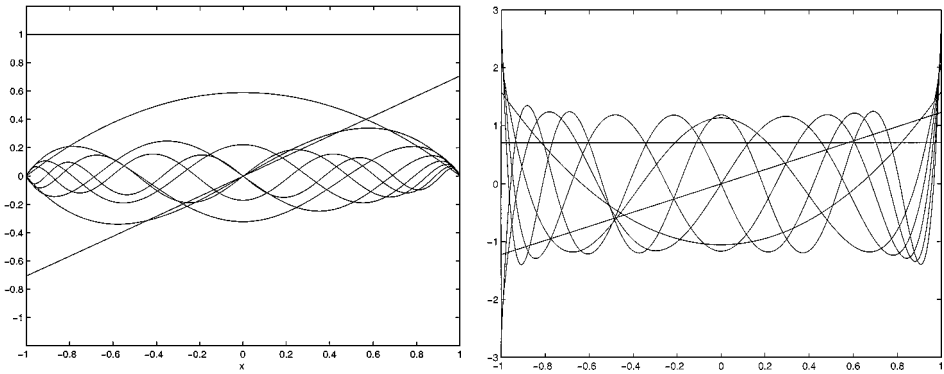

FIG. 1. Left: functions of the Legendre basis $L_n^*(x)$, $n = 0, 1, 2, \ldots$, for Dirichlet boundary conditions. Right: functions of the Legendre basis $L_{\hat{n}}^{\diamond}(x)$, $\hat{n} = 0, 1, 2, \ldots$, for natural boundary conditions.

Since the velocity field satisfies Dirichlet conditions, we adopt the basis introduced by Jie Shen in [34],

$$\begin{aligned} L_0^*(x) &= 1 \\ L_1^*(x) &= \frac{x}{\sqrt{2}} \\ L_n^*(x) &= \frac{L_{n-2}(x) - L_n(x)}{\sqrt{2(2n-1)}}, \quad n \geq 2, \end{aligned} \tag{2.2}$$

where $L_n(x)$, $n \geq 0$, are Legendre polynomials. This basis includes the first two modes for imposing nonhomogeneous Dirichlet conditions by means of a (numerical) lifting described in details in [3]. In practice we have

$$\boldsymbol{X}_{0,N} = [\text{span}\{L_m^*(x)L_n^*(y) : 2 \leq m \leq N, 2 \leq n \leq N\}]^2. \tag{2.3}$$

The first few functions $L_n^*(x)$ are shown on the left in Fig. 1. This basis generates sparse stiffness and mass matrices. More specifically, the restriction to $\boldsymbol{X}_{0,N}$ of the stiffness matrix is the identity matrix, while the mass matrix is pentadiagonal symmetric with only three codiagonals different from zero. The nonzero elements of the mass matrix are given in [3] and [34].

As far as the pressure approximation is concerned, since this unknown in the fractional step projection method satisfies Neumann boundary conditions, a convenient basis for the two-dimensional problem is obtained by the direct product of the standard Legendre polynomials. This basis is normalized so as to obtain a mass matrix coincident with the identity matrix:

$$L_{\hat{n}}^{\diamond}(x) = \sqrt{\hat{n} + \tfrac{1}{2}}\, L_{\hat{n}}(x), \quad \hat{n} \geq 0. \tag{2.4}$$

The first few functions $L_{\hat{n}}^{\diamond}(x)$ of the basis for Neumann conditions are shown on the right in Fig. 1. In this basis, the mass matrix is simply the identity while the stiffness matrix is full, and is evaluated exactly (within roundoff error) by means of the Gauss–Legendre numerical quadrature.

The velocity and pressure fields representing the approximate solution to the Navier–Stokes problem (2.1) are expanded in the double series,

$$\boldsymbol{u}_N(t,x,y) = \sum_{n=2}^{N} L_n^*(x)\, \boldsymbol{U}_{n,m}(t)\, L_m^*(y), \sum_{m=2}^{N}, \tag{2.5}$$

$$p_{\hat{N}}(t,x,y) = \sum_{\hat{n}=0}^{\hat{N}} L_{\hat{n}}^{\diamond}(x)\, P_{\hat{n},\hat{m}}(t)\, L_{\hat{m}}^{\diamond}(y), \sum_{\hat{m}=0}^{\hat{N}}, \tag{2.6}$$

where the symbol $\sum$ is used to distinguish the summation on the second index from the summation on the first one, following the notation proposed in [3]. This manner of indicating the two different summations is particularly convenient to represent the action of spatial differential operators along the directions x and y. In fact, the corresponding one-dimensional operators are represented by square matrices that pre- and postmultiply the arrays $\boldsymbol{U}$ and P of the Legendre coefficients of velocity and pressure.

The choice of the two different bases for velocity and pressure is motivated on the one hand by the need to impose essential boundary conditions for the viscous step and natural boundary conditions for the projection step, and on the other hand, by the aim to retain in both cases the tensor product structure of the elliptic solvers, as will be made clear in the following sections.

2.3. Semi-discrete Weak Spectral Equations

The approximate semi-discrete Navier–Stokes problem in weak form is the following. For $t \geq 0$, find $\boldsymbol{u}_N \in C^1([0,T]; \boldsymbol{X}_{0,N})$, $p_{\hat{N}} \in C^0([0,T]; M_{\hat{N}})$ such that, for all $\boldsymbol{v}_N \in \boldsymbol{X}_{0,N}$ and all $q_{\hat{N}} \in M_{\hat{N}}$,

$$\begin{cases} \big(\boldsymbol{v}_N, \boldsymbol{u}_N(t=0)\big) = \big(\boldsymbol{v}_N, \boldsymbol{u}_0\big) \\ \left(\boldsymbol{v}_N, \dfrac{\partial \boldsymbol{u}_N}{\partial t}\right) + \nu\big(\boldsymbol{\nabla}\boldsymbol{v}_N, \boldsymbol{\nabla}\boldsymbol{u}_N\big) + \big(\boldsymbol{v}_N, (\boldsymbol{u}_N \cdot \boldsymbol{\nabla})\boldsymbol{u}_N\big) + \big(\boldsymbol{v}_N, \boldsymbol{\nabla} p_{\hat{N}}\big) = \big(\boldsymbol{v}_N, \boldsymbol{f}\big)_N \\ \big(q_{\hat{N}}, \boldsymbol{\nabla}\cdot\boldsymbol{u}_N\big) = 0, \end{cases} \tag{2.7}$$

where $(\cdot,\cdot)$ denotes the $L^2(\Omega)$ inner product, while $(\cdot,\cdot)_N$ indicates a suitable approximation of the $L^2(\Omega)$ inner product for the source term, evaluated by means of a Gauss–Legendre quadrature formula.

It is known that the well posedness of the discrete problem depends on the satisfaction of a compatibility condition between the approximation spaces for the velocity and the pressure, called *inf-sup* condition or LBB compatibility condition from Ladyzhenskaya, Babuška and Brezzi [7, 12, 29]. In this work, the *inf-sup* condition has been satisfied by assuming $\hat{N} = N - 2$, indeed we have the following result (see Bernardi and Maday [9]):

LEMMA. *When $\hat{N} = N - 2$, there is $\beta > 0$ such that*

$$\forall q_{\hat{N}} \in M_{\hat{N}}, \quad \exists \boldsymbol{v}_N \in \boldsymbol{X}_{0,N}, \boldsymbol{v}_N \neq \boldsymbol{0}: \quad (q_{\hat{N}}, \boldsymbol{\nabla}\cdot\boldsymbol{v}_N) \geq \beta N^{-1/2} \|q_{\hat{N}}\|_0 \|\boldsymbol{v}_N\|_{\boldsymbol{H}^1(\Omega)}. \tag{2.8}$$

If the fields $\boldsymbol{u}(\cdot,t)$ and $p(\cdot,t)$, exact solution of problem (2.1), own the regularity of $\boldsymbol{H}^\sigma(\Omega)$ and $H^{\sigma-1}(\Omega)$, respectively, $\sigma \geq 1$, then the solution $(\boldsymbol{u}_N, p_{\hat{N}})$ of the weak approximate problem (2.7) converges to the exact solution with a rate equal to σ (resp. $\sigma - 1$) in the L^2 (resp. H^1) norm, as stated by the following estimates:

THEOREM. *When* $\hat{N} = N - 2$, *we have*

$$\|\boldsymbol{u} - \boldsymbol{u}_N\|_{L^\infty(0,T;\boldsymbol{L}^2(\Omega))} \le cN^{-\sigma}\left\{\|\boldsymbol{u}\|_{W^{1,\infty}(0,T;\boldsymbol{H}^\sigma(\Omega))} + \|p\|_{W^{1,\infty}(0,T;H^{\sigma-1}(\Omega))}\right\}, \tag{2.9}$$

and

$$\begin{aligned}\|\boldsymbol{u} - \boldsymbol{u}_N\|_{L^\infty(0,T;\boldsymbol{H}^1(\Omega))} + N^{-1/2}\|p - p_{\hat{N}}\|_{L^\infty(0,T;L^2(\Omega))} \\ \le cN^{1-\sigma}\left\{\|\boldsymbol{u}\|_{W^{1,\infty}(0,T;\boldsymbol{H}^\sigma(\Omega))} + \|p\|_{W^{1,\infty}(0,T;H^{\sigma-1}(\Omega))}\right\}.\end{aligned} \tag{2.10}$$

In this theorem, $H^s(\Omega)$ ($\boldsymbol{H}^s(\Omega)$) denotes the Sobolev space of scalar (vector) functions which are square integrable over Ω and whose derivatives are also square integrable over Ω up to order s; $W^{1,\infty}(0, T; H^s(\Omega))$ denotes the space of functions which are absolutely integrable in any power, together with their first time derivative, on the interval $(0, T)$ and are $H^s(\Omega)$ in space for each time in $(0, T)$.

3. THE SECOND-ORDER BDF SPECTRAL PROJECTION METHOD

The projection method is a time-marching algorithm composed of two separate substeps aiming at decoupling the effect of viscosity from the incompressibility constraint. At each time step, an intermediate velocity is computed by advancing in time the momentum equation with the pressure gradient term omitted. The end-of-step velocity is then obtained by projecting such an intermediate velocity onto the space of divergence-free vector fields with zero normal component on the boundary and determining an approximation of the pressure field. The incremental version of the projection method (also known as pressure correction method) consists in making explicit the pressure at the viscous step and correcting it at the projection step, while still retaining the complete uncoupling of viscous diffusion from incompressibility constraint.

According to the theoretical analysis given in [21], the incremental version, using a Galerkin spatial approximation and a first-order Euler time stepping, is more accurate than the nonincremental one for any value of the time step. In fact, the incremental fractional-step method is characterized by a time-splitting error of $\mathcal{O}((\Delta t)^2)$. This property can be exploited in order to develop a second-order projection method by introducing a suitable second-order accurate time discretization.

In this work, we consider the scheme based on the second order BDF (Backward Difference Formula), which has been introduced and studied thoroughly by Guermond [19]. Here this scheme is applied in the context of the proposed Galerkin–Legendre spatial approximation.

3.1. BDF Incremental Time Discretization

For generality of the final solution algorithm, hereafter we consider nonhomogeneous boundary conditions for the velocity of the form $\boldsymbol{u}_{|\partial\Omega} = \boldsymbol{b}$, where the velocity datum $\boldsymbol{b}$ is assumed to satisfy the global incompressibility constraint $\int_{\partial\Omega} \boldsymbol{n} \cdot \boldsymbol{b} = 0$.

Using k to denote the time index, two sequences of approximate velocities $(\boldsymbol{u}^k)_{k\ge0}$ and $(\hat{\boldsymbol{u}}^k)_{k\ge1}$ are sought for. We set now $\boldsymbol{u}^0 = \boldsymbol{u}_0$ and assume that an initial pressure field P^0

is available or can be evaluated as the steady state[1] pressure associated with the initial velocity $\boldsymbol{u}_0$.

Let us consider the time steps for $k \geq 1$, leaving the first step, $k = 0$, for later discussion. The BDF incremental projection method consists in solving the following two problems.

First, consider the diffusion step

$$\begin{cases} \dfrac{3\boldsymbol{u}^{k+1} - 4i^{\mathrm{tr}}\hat{\boldsymbol{u}}^{k} + i^{\mathrm{tr}}\hat{\boldsymbol{u}}^{k-1}}{2\Delta t} - \nu\nabla^2\boldsymbol{u}^{k+1} = \boldsymbol{f}^{k+1} - (\boldsymbol{u}_\star^{k+1}\cdot\boldsymbol{\nabla})\boldsymbol{u}_\star^{k+1} - \boldsymbol{\nabla}p^{k}, \\ \boldsymbol{u}^{k+1}|_{\partial\Omega} = \boldsymbol{b}^{k+1}, \end{cases} \tag{3.1}$$

where we have introduced the linearly extrapolated velocity $\boldsymbol{u}_\star^{k+1} = 2\boldsymbol{u}^{k} - \boldsymbol{u}^{k-1}$.

Then, perform the projection step in the following second-order incremental form:

$$\begin{cases} \dfrac{3}{2}\dfrac{\hat{\boldsymbol{u}}^{k+1} - i\boldsymbol{u}^{k+1}}{\Delta t} + \hat{\boldsymbol{\nabla}}(p^{k+1} - p^{k}) = 0, \\ \hat{\boldsymbol{\nabla}}\cdot\hat{\boldsymbol{u}}^{k+1} = 0, \\ \boldsymbol{n}\cdot\hat{\boldsymbol{u}}^{k+1}|_{\partial\Omega} = \boldsymbol{n}\cdot\boldsymbol{b}^{k+1}. \end{cases} \tag{3.2}$$

In the projection step (3.2) appears the injection operator i from $\boldsymbol{H}_0^1(\Omega)$ into the space

$$\boldsymbol{H}_0^{\mathrm{div}}(\Omega) = \{\hat{\boldsymbol{v}} \in \boldsymbol{L}^2(\Omega) \mid \hat{\boldsymbol{\nabla}}\cdot\hat{\boldsymbol{v}} \in L^2(\Omega), \boldsymbol{n}\cdot\hat{\boldsymbol{v}}|_{\partial\Omega} = 0\},$$

which has the correct regularity for the velocity field obtained in the (inviscid) projection step. Correspondingly, in the viscous problem (3.1) there is the transpose operator i^{tr}. The expression $\hat{\boldsymbol{\nabla}}\cdot : \boldsymbol{H}_0^{\mathrm{div}}(\Omega) \to L^2(\Omega)$ is an extension of $\boldsymbol{\nabla}\cdot : \boldsymbol{H}_0^1(\Omega) \to L^2(\Omega)$ in the sense that we have the remarkable property:

$$\hat{\boldsymbol{\nabla}}\cdot i = \boldsymbol{\nabla}\cdot \quad \text{and} \quad i^{\mathrm{tr}}\hat{\boldsymbol{\nabla}} = \boldsymbol{\nabla}.$$

This distinction may seem unduly pedantic in the context of the spatially continuous problem, but it proves to be of the utmost importance when it comes to discretizing the equations in space; for details see [21].

By applying $\hat{\boldsymbol{\nabla}}\cdot$ to the first equation of (3.2), we obtain the following Neumann problem for the Poisson equation for the increment $(p^{k+1} - p^{k})$,

$$\begin{cases} -\hat{\nabla}^2(p^{k+1} - p^{k}) = -\frac{3}{2\Delta t}\boldsymbol{\nabla}\cdot\boldsymbol{u}^{k+1}, \\ \left.\dfrac{\partial(p^{k+1} - p^{k})}{\partial n}\right|_{\partial\Omega} = 0, \end{cases} \tag{3.3}$$

where we have used $\hat{\boldsymbol{\nabla}}\cdot i = \boldsymbol{\nabla}\cdot$.

In the first time step ($k = 0$), the incremental projection scheme based on the two-level Euler time discretization is exploited to determine the first velocity $\boldsymbol{u}^1$ and pressure p^1. This

[1] This assumption breaks down in the case of an impulsive start whenever $\boldsymbol{n}\cdot\boldsymbol{b} \neq 0$ at the initial time on (part of) the boundary; for details see [32, Section 1.2].

means solving the viscous diffusion problem

$$\begin{cases} \dfrac{\boldsymbol{u}^1 - \boldsymbol{u}^0}{\Delta t} - \nu \nabla^2 \boldsymbol{u}^1 = \boldsymbol{f}^1 - (\boldsymbol{u}^0 \cdot \boldsymbol{\nabla})\boldsymbol{u}^0 - \boldsymbol{\nabla} p^0, \\ \qquad\qquad \boldsymbol{u}^1|_{\partial\Omega} = \boldsymbol{b}^1, \end{cases} \tag{3.4}$$

and the incremental Poisson problem

$$\begin{cases} -\hat{\nabla}^2 (p^1 - p^0) = -(\Delta t)^{-1} \boldsymbol{\nabla} \cdot \boldsymbol{u}^1, \\ \left. \dfrac{\partial (p^1 - p^0)}{\partial n} \right|_{\partial\Omega} = 0, \end{cases} \tag{3.5}$$

so that the first end-of-step velocity is given by $\hat{\boldsymbol{u}}^1 = i\boldsymbol{u}^1 - \Delta t \hat{\boldsymbol{\nabla}}(p^1 - p^0)$.

As anticipated, the end-of-step velocity can be profitably eliminated from the algorithm. The elimination in the BDF method requires paying special attention to the two steps with $k = 1$ and $k = 2$. In fact, the first end-of-step velocity is $\hat{\boldsymbol{u}}^1 = i\boldsymbol{u}^1 - \Delta t \hat{\boldsymbol{\nabla}}(p^1 - p^0)$ and its elimination gives expressions for the extrapolated pressure in the second and third time steps $k = 1$ and $k = 2$ different from that valid at all other subsequent time steps with $k \geq 3$. A direct calculation leads to the following equation of the viscous step for $k \geq 1$, with the end-of-step velocity eliminated,

$$\begin{aligned} &\frac{3\boldsymbol{u}^{k+1} - 4\boldsymbol{u}^k + \boldsymbol{u}^{k-1}}{2\Delta t} - \nu \nabla^2 \boldsymbol{u}^{k+1} = \boldsymbol{f}^{k+1} - (\boldsymbol{u}_\star^{k+1} \cdot \boldsymbol{\nabla})\boldsymbol{u}_\star^{k+1} \\ &\quad - \begin{cases} \boldsymbol{\nabla}(3p^1 - 2p^0) & \text{if } k = 1 \\ \frac{1}{6}\boldsymbol{\nabla}(14p^2 - 11p^1 + 3p^0) & \text{if } k = 2 \\ \frac{1}{3}\boldsymbol{\nabla}(7p^k - 5p^{k-1} + p^{k-2}) & \text{if } k \geq 3 \end{cases} \\ &\qquad\qquad \boldsymbol{u}^{k+1}|_{\partial\Omega} = \boldsymbol{b}^{k+1}. \end{aligned} \tag{3.6}$$

3.2. Fully Discrete Equations

By introducing the finite dimensional spaces $\boldsymbol{X}_{0,N}$ and $M_{\hat{N}}$, we recast the BDF incremental projection algorithm in weak form. The nonhomogeneous Dirichlet condition for the velocity is taken into account by means of a lifting described thoroughly in [3]. This means that the solution $\boldsymbol{u}_N^{k+1}$ is expressed in the form

$$\boldsymbol{u}_N^{k+1} = \boldsymbol{u}_{\boldsymbol{b}^{k+1},N} + \boldsymbol{u}_{0,N}^{k+1}. \tag{3.7}$$

Here, the first term $\boldsymbol{u}_{\boldsymbol{b}^{k+1},N} \in \boldsymbol{X}_N$ and is such that $\boldsymbol{u}_{\boldsymbol{b}^{k+1},N|\partial\Omega} \approx \boldsymbol{b}^{k+1}$ in the sense of the $L^2(\partial\Omega)$ projection (but for the corner values, which are imposed exactly) while the second term $\boldsymbol{u}_{0,N}^{k+1}$ belongs to $\boldsymbol{X}_{0,N}$ and satisfies the equation governing $\boldsymbol{u}_N^{k+1}$ with the right-hand side perturbed by the lifting. The latter is implemented numerically through the "extended" mass matrix M^*; for details see [3].

Considering, for instance, the general viscous step valid for $k \geq 3$, we have the weak problem:

For $k \geq 3$, find $\boldsymbol{u}_{0,N}^{k+1} \in \boldsymbol{X}_{0,N}$ such that, for all $\boldsymbol{v}_N \in \boldsymbol{X}_{0,N}$,

$$\begin{aligned}\left(\boldsymbol{v}_N, \frac{3\boldsymbol{u}_{0,N}^{k+1} - 4\boldsymbol{u}_N^k + \boldsymbol{u}_N^{k-1}}{2\Delta t}\right) + \nu\left(\boldsymbol{\nabla}\boldsymbol{v}_N, \boldsymbol{\nabla}\boldsymbol{u}_{0,N}^{k+1}\right) \\ = -\frac{3}{2\Delta t}\left(\boldsymbol{v}_N, \boldsymbol{u}_{\boldsymbol{b}^{k+1},N}\right) - \nu\left(\boldsymbol{\nabla}\boldsymbol{v}_N, \boldsymbol{\nabla}\boldsymbol{u}_{\boldsymbol{b}^{k+1},N}\right) + \left(\boldsymbol{v}_N, \boldsymbol{f}^{k+1}\right)_N \\ - \left(\boldsymbol{v}_N, (\boldsymbol{u}_{\star,N}^{k+1}\cdot\boldsymbol{\nabla})\boldsymbol{u}_{\star,N}^{k+1}\right) - \frac{1}{3}\left(\boldsymbol{v}_N, \boldsymbol{\nabla}\left(7p_{\hat{N}}^k - 5p_{\hat{N}}^{k-1} + p_{\hat{N}}^{k-2}\right)\right).\end{aligned} \tag{3.8}$$

Still choosing $\boldsymbol{X}_N + \hat{\boldsymbol{\nabla}} M_{\hat{N}}$ as the functional space for the end-of-step velocity, $\hat{\boldsymbol{u}}^{k+1}$, the weak form of the projection step of the BDF method reads:

For $k \geq 1$, find $(p_{\hat{N}}^{k+1} - p_{\hat{N}}^k) \in M_{\hat{N}}$ such that, for all $q_{\hat{N}} \in M_{\hat{N}}$,

$$\left(\hat{\boldsymbol{\nabla}} q_{\hat{N}}, \hat{\boldsymbol{\nabla}}\left(p_{\hat{N}}^{k+1} - p_{\hat{N}}^k\right)\right) = -\frac{3}{2\Delta t}\left(q_{\hat{N}}, \boldsymbol{\nabla}\cdot\boldsymbol{u}_N^{k+1}\right). \tag{3.9}$$

Introducing $L_n^*(x)L_m^*(y)$, $2 \leq (n,m) \leq N$, [resp. $L_{\hat{N}}^\diamond(x)L_{\hat{m}}^\diamond(y)$, $0 \leq (\hat{n},\hat{m}) \leq \hat{N}$] as test functions in Eq. (3.8) [resp. (3.9)] the two substeps are expressed in matrix form as

$$\boldsymbol{U}_0^{k+1}M^* + M^*\boldsymbol{U}_0^{k+1} + \gamma M^*\boldsymbol{U}_0^{k+1}M^* = \boldsymbol{F}^{k+1}, \tag{3.10}$$

$$D^\diamond(P^{k+1} - P^k) + (P^{k+1} - P^k)D^\diamond = G^{k+1}, \tag{3.11}$$

where $\gamma = 3/(2\nu\Delta t)$. In Eq. (3.10) M^* is the mass matrix associated with the basis L_n^*, $n = 0,\ldots,N$ and, similarly, in Eq. (3.11) $D^\diamond$ is the stiffness matrix associated with the basis $L_{\hat{n}}^*$, $\hat{n} = 0,\ldots,\hat{N}$. Because of the symmetry of M^* and $D^\diamond$, we have not indicated the transposition of matrices that multiply on the right.

The right-hand sides of the two Eqs. (3.10) and (3.11) are defined, respectively, by

$$\begin{aligned}\nu\boldsymbol{F}_{n,m}^{k+1} = {} & \frac{1}{2\Delta t}\left(L_n^*(x)L_m^*(y), 4\boldsymbol{u}_N^k - \boldsymbol{u}_N^{k-1}\right) + \left(L_n^*(x)L_m^*(y), \boldsymbol{f}^{k+1}\right)_N \\ & - \frac{3}{2\Delta t}\left(L_n^*(x)L_m^*(y), \boldsymbol{u}_{\boldsymbol{b}^{k+1},N}\right) - \nu\left(L_n^{*\prime}(x)L_m^*(y), \frac{\partial \boldsymbol{u}_{\boldsymbol{b}^{k+1},N}}{\partial x}\right) \\ & - \nu\left(L_n^*(x)L_m^{*\prime}(y), \frac{\partial \boldsymbol{u}_{\boldsymbol{b}^{k+1},N}}{\partial y}\right) - \frac{1}{3}\left(L_n^*(x)L_m^*(y), \boldsymbol{\nabla}\left(7p_{\hat{N}}^k - 5p_{\hat{N}}^{k-1} + p_{\hat{N}}^{k-2}\right)\right) \\ & - \left(L_n^*(x)L_m^*(y), (\boldsymbol{u}_{\star,N}^{k+1}\cdot\boldsymbol{\nabla})\boldsymbol{u}_{\star,N}^{k+1}\right),\end{aligned} \tag{3.12}$$

$$G_{\hat{n},\hat{m}}^{k+1} = -\frac{3}{2\Delta t}\left(L_{\hat{n}}^\diamond(x)L_{\hat{m}}^\diamond(y), \boldsymbol{\nabla}\cdot\boldsymbol{u}_N^{k+1}\right). \tag{3.13}$$

The evaluation of the terms involving the pressure gradient and the velocity divergence requires the computation of integrals associated with "hybrid" scalar products of the type $\left(L_n^*(x), L_{\hat{n}}^{\diamond\prime}(x)\right)$ and $\left(L_{\hat{n}}^\diamond(x), L_n^{*\prime}(x)\right)$, respectively. Moreover, these terms require also the computation of "hybrid" mass matrices of the type $\left(L_n^*(x), L_{\hat{n}}^\diamond(x)\right)$ and $\left(L_{\hat{n}}^\diamond(x), L_n^*(x)\right)$. The profiles and elements of all these matrices will be given in Section 4.1. The nonlinear terms are evaluated by means of the pseudospectral technique based here on the Gauss–Legendre quadrature and resorting to the $3N/2$ rule to ensure exact integration of the quadratic nonlinearities, as described in Section 4.2.

The solution of the algebraic systems (3.10) for the velocity components is obtained by means of a direct fast Helmholtz solver based on the eigen-decomposition of the mass matrices in the two spatial directions; see [3], and [4] for the 3D case. The solution of the pressure system (3.11) is obtained by an analogous fast spectral Poisson solver which imposes the boundary condition in the standard natural way and is based on the eigen-decomposition of the stiffness matrices.

4. GALERKIN–LEGENDRE MATRICES AND PSEUDOSPECTRAL TECHNIQUE

In this section we provide the explicit expressions of the various "hybrid" matrices, i.e., involving scalar products of pairs of functions belonging to the two different bases, that occurr in the right-hand sides (3.12) and (3.13) of the algebraic systems of equations for velocity (3.10) and pressure (3.11).

Moreover, we detail how to evaluate the nonlinear terms by means of a pseudospectral technique ensconced in the integration points of Gauss–Legendre quadrature formulas.

4.1. Hybrid Matrices

Let us now consider the various hybrid matrices needed to evaluate the right-hand sides of the momentum and pressure equations (3.12) and (3.13). The linear terms involving the gradient and the divergence are rewritten here as

$$\begin{Bmatrix} H^x_{n,m} \\ H^y_{n,m} \end{Bmatrix} = \left(L^*_n(x)L^*_m(y), \boldsymbol{\nabla} q_{\hat{N}}\right),$$

and

$$G_{\hat{n},\hat{m}} = \left(L^\diamond_{\hat{n}}(x)L^\diamond_{\hat{m}}(y), \boldsymbol{\nabla}\cdot u_N\right).$$

We first consider the x-component of the term associated with the pressure gradient, namely,

$$H^x_{n,m} = \sum_{\hat{n}=0}^{\hat{N}} a^{*\diamond}_{n,\hat{n}}, \delta P_{\hat{n},\hat{m}}, m^{*\diamond}_{\hat{m},m} \sum_{\hat{m}=0}^{\hat{N}},$$

where we introduced the hybrid (in general rectangular) matrices $A^{*\diamond}$ and $M^{*\diamond}$ with elements defined by

$$a^{*\diamond}_{n,\hat{n}} \equiv \int_{-1}^{1} L^*_n(x)L^{\diamond\prime}_{\hat{n}}(x)\,dx, \qquad 0 \le n \le N, 0 \le \hat{n} \le \hat{N},$$

$$m^{*\diamond}_{n,\hat{n}} \equiv \int_{-1}^{1} L^*_n(x)L^\diamond_{\hat{n}}(x)\,dx, \qquad 0 \le n \le N, 0 \le \hat{n} \le \hat{N}.$$

In matrix form, the contribution to the right-hand side of the velocity equation resulting from the pressure gradient reads

$$H^x = A^{*\diamond}\delta P(M^{*\diamond})^T \quad \text{and} \quad H^y = M^{*\diamond}\delta P(A^{*\diamond})^T,$$

where the superscript T denotes the transposed matrix.

The matrices $A^{*\diamond}$ and $M^{*\diamond}$ display a sparse profile and their nonzero elements can be evaluated in closed form. For instance, the generic element of $M^{*\diamond}$, for $n \ge 2$ and $\hat{n} \ge 2$, is

defined by

$$m^{*\diamond}_{n,\hat{n}} = (L^*_n, L^\diamond_{\hat{n}}) = \left(\frac{L_{n-2} - L_n}{\sqrt{2(2n-1)}}, k(\hat{n}) L_{\hat{n}} \right),$$

where $k(\hat{n}) = \hat{n} + \frac{1}{2}$. Thanks to the orthogonality of Legendre polynomials, the only elements of $M^{*\diamond}$ different from zero lie on the diagonals $n = \hat{n}$ or $n = \hat{n} + 2$; in fact,

$$m^{*\diamond}_{\hat{n},\hat{n}} = -\sqrt{\frac{\hat{n}+\frac{1}{2}}{2(2\hat{n}-1)}} \frac{1}{\hat{n}+\frac{1}{2}} = -\frac{1}{\sqrt{4\hat{n}^2-1}}, \quad \hat{n} \geq 2,$$

$$m^{*\diamond}_{\hat{n}+2,\hat{n}} = \sqrt{\frac{\hat{n}+\frac{1}{2}}{2(2\hat{n}+3)}} \frac{1}{\hat{n}+\frac{1}{2}} = \frac{1}{\sqrt{(2\hat{n}+1)(2\hat{n}+3)}}, \quad \hat{n} \geq 2.$$

Thus, matrix $M^{*\diamond}$ is tridiagonal with only two diagonals different from zero

$$M^{*\diamond} = \begin{array}{c} \\ 0 \\ 1 \\ 2 \\ \vdots \\ N-2 \\ N-1 \\ N \end{array} \begin{array}{c} \begin{array}{cccccc} 0 & \cdots & \cdots & \cdots & \hat{N} \end{array} \\ \begin{pmatrix} b_0 & & & & \\ 0 & b_1 & & & \\ a_0 & 0 & \ddots & & \\ & a_1 & \ddots & \ddots & \\ & & \ddots & \ddots & b_{\hat{N}} \\ & & & \ddots & 0 \\ & & & & a_{\hat{N}} \end{pmatrix} \end{array},$$

where

$$a_0 = \frac{1}{\sqrt{3}}, \qquad a_n = \frac{1}{\sqrt{(2n+1)(2n+3)}}, \quad n \geq 1,$$

$$b_0 = \sqrt{2}, \qquad b_n = -\frac{1}{\sqrt{4n^2-1}}, \quad n \geq 1.$$

To calculate the elements of $A^{*\diamond}$, it is useful to proceed by integrating by parts the generic element, so that, being $L^*_n(\pm 1) = 0$ if $n > 2$, we have, for $n \geq 2$ and $\hat{n} \geq 0$,

$$a^{*\diamond}_{n,\hat{n}} = \left(L^*_n, L^{\diamond\prime}_{\hat{n}}\right) = -\left(L^{*\prime}_n, L^\diamond_{\hat{n}}\right) + \left[L^*_n L^\diamond_{\hat{n}}\right]\Big|^1_{-1} = -\left(L^{*\prime}_n, L^\diamond_{\hat{n}}\right).$$

Using the properties of Legendre polynomials [36], we obtain

$$a^{*\diamond}_{n,\hat{n}} = -\left(\frac{\sqrt{n-\frac{1}{2}}}{n(n-1)} \frac{d}{dx} \left[(1-x^2) \frac{dL_n(x)}{dx} \right], L^\diamond_{\hat{n}}(x) \right) = \left(\sqrt{n-\frac{1}{2}} L_{n-1}, k(\hat{n}) L_{\hat{n}} \right),$$

which is different from zero only on the diagonal corresponding to $n = \hat{n} + 1$,

$$a^{*\diamond}_{\hat{n}+1,\hat{n}} = \frac{\sqrt{\hat{n}+\frac{1}{2}}\sqrt{\hat{n}+\frac{1}{2}}}{\hat{n}+\frac{1}{2}} = 1, \quad \hat{n} \geq 1.$$

The elements belonging to the first two rows are defined, for $1 \le \hat{n} \le \hat{N}$, by

$$a^{*\diamond}_{0,\hat{n}} = -\left(L^{*\prime}_0, L^{\diamond}_{\hat{n}}\right) + \left[L^{*}_0 L^{\diamond}_{\hat{n}}\right]\Big|^{1}_{-1} = \left[k(\hat{n}) L_{\hat{n}}\right]\Big|^{1}_{-1},$$
$$a^{*\diamond}_{1,\hat{n}} = -\left(L^{*\prime}_1, L^{\diamond}_{\hat{n}}\right) + \left[L^{*}_1, L^{\diamond}_{\hat{n}}\right]\Big|^{1}_{-1} = \frac{1}{\sqrt{2}}\left[x k(\hat{n}) L_{\hat{n}}\right]\Big|^{1}_{-1}.$$

For the parity properties of Legendre polynomials, we have, for $\hat{n} \ge 1$,

$$a^{*\diamond}_{0,\hat{n}} = \begin{cases} 0, & \hat{n} \text{ even} \\ -\left(\hat{n} + \frac{1}{2}\right), & \hat{n} \text{ odd} \end{cases} \qquad \text{and} \qquad a^{*\diamond}_{1,\hat{n}} = \begin{cases} 0, & \hat{n} \text{ odd} \\ -\sqrt{2}\left(\hat{n} + \frac{1}{2}\right), & \hat{n} \text{ even} \end{cases}$$

Therefore, matrix $A^{*\diamond}$ presents the following structure,

$$A^{*\diamond} = \begin{array}{c} \\ 0 \\ 1 \\ 2 \\ \vdots \\ N-1 \\ N \end{array} \begin{array}{c} \begin{array}{cccc} 0 & 1 & \cdots & \hat{N} \end{array} \\ \begin{pmatrix} d_0 & d_1 & \dots & d_{\hat{N}} \\ c_0 & c_1 & \dots & c_{\hat{N}} \\ & 1 & & \\ & & \ddots & \\ & & & 1 \end{pmatrix} \end{array},$$

where

$$d_n = 0, \quad n \text{ even}; \qquad d_n = 2\sqrt{n + \frac{1}{2}}, \quad n \text{ odd};$$
$$c_0 = 0, \quad c_n = 0, \quad n \text{ odd}; \qquad c_n = \sqrt{2n+1}, \quad n \text{ even} \ge 2.$$

The evaluation of the right-hand side for the pressure problem is obtained in an analogous way. In fact

$$\begin{aligned} G_{\hat{n},\hat{m}} &= \sum_{n=0}^{N} \int_{-1}^{1} L^{\diamond}_{\hat{n}}(x) L^{*\prime}_{n}(x)\, dx\, U_{n,m} \int_{-1}^{1} L^{*}_{m}(y) L^{\diamond}_{\hat{m}}(y)\, dy \sum_{m=0}^{N} \\ &\quad + \sum_{n=0}^{N} \int_{-1}^{1} L^{\diamond}_{\hat{n}}(x) L^{*}_{n}(x)\, dx\, V_{n,m} \int_{-1}^{1} L^{*\prime}_{m}(y) L^{\diamond}_{\hat{m}}(y)\, dy \sum_{m=0}^{N} \\ &= \sum_{n=0}^{N} b^{\diamond *}_{\hat{n},n}, U_{n,m}, m^{*\diamond}_{m,\hat{m}}, \sum_{m=0}^{N} + \sum_{n=0}^{N} m^{*\diamond}_{n,\hat{n}}, V_{n,m}, b^{\diamond *}_{\hat{m},m}, \sum_{m=0}^{N}, \end{aligned}$$

where $(U, V) = \boldsymbol{U}$ and where the coefficients

$$b^{\diamond *}_{\hat{n},n} \equiv \int_{-1}^{1} L^{\diamond}_{\hat{n}}(x) L^{*\prime}_{n}(x)\, dx, \qquad 0 \le \hat{n} \le \hat{N}, 0 \le n \le N,$$

define the hybrid matrix $B^{\diamond *}$ which has the following structure:

$$B^{\diamond *} = \begin{array}{c} \\ 0 \\ 1 \\ \vdots \\ \hat{N} \end{array} \begin{array}{c} \begin{array}{cccccc} 0 & 1 & 2 & \cdots & N-1 & N \end{array} \\ \begin{pmatrix} & & & & & \\ & 1 & & & & \\ & & -1 & & & \\ & & & \ddots & & \\ & & & & -1 & \end{pmatrix} \end{array}.$$

The proof of this result is identical, up to the sign, to the one described for $A^{*\diamond}$.

Therefore, the right-hand side for the pressure problem, formulated in matrix form, reads

$$G = -\frac{1}{\Delta t}\left[B^{\diamond *} U M^{*\diamond} + (M^{*\diamond})^T V (B^{\diamond *})^T\right].$$

4.2. Pseudospectral Evaluation of the Nonlinear Term

The nonlinear term is evaluated according to Orszag's pseudospectral technique. We first consider the nonlinear term $c_N(x, y) = \boldsymbol{u}_N \cdot \boldsymbol{\nabla} u_N$ for the momentum equation in x direction, expressed in weak formulation,

$$C_{n,m} = \left(L_n^*(x) L_m^*(y), c_N(x, y)\right) = \left(L_n^*(x) L_m^*(y), u_N \frac{\partial u_N}{\partial x}\right) + \left(L_n^*(x) L_m^*(y), v_N \frac{\partial u_N}{\partial y}\right),$$

where $\boldsymbol{u} = u\hat{\boldsymbol{x}} + v\hat{\boldsymbol{y}}$.

To determine the values $C_{n,m}$ of the L^2 projection of $c_N(x, y)$, one introduces first the point values of the solution u_N and v_N at the $\frac{3}{2}(N+1) \times \frac{3}{2}(N+1)$ Gauss–Legendre points in the square $[-1,\ 1]^2$, as follows

$$u_N(x, y) \to \mathcal{U} \equiv \left\{u_N(x_h, y_k), 1 \le (h, k) \le \frac{3}{2}(N+1)\right\},$$

$$v_N(x, y) \to \mathcal{V} \equiv \left\{v_N(x_h, y_k), 1 \le (h, k) \le \frac{3}{2}(N+1)\right\},$$

and, similarly, the point values of the derivatives of u_N at the Gauss–Legendre integration points

$$\mathcal{U}_{(x)} \equiv \left\{\frac{\partial u_N(x_h, y_k)}{\partial x}, 1 \le (h, k) \le \frac{3}{2}(N+1)\right\},$$

$$\mathcal{U}_{(y)} \equiv \left\{\frac{\partial u_N(x_h, y_k)}{\partial y}, 1 \le (h, k) \le \frac{3}{2}(N+1)\right\}.$$

All these point values can be evaluated from the Legendre coefficient arrays U and V by means of

$$\mathcal{U} = \mathcal{L}^* U \mathcal{L}^{*T}, \quad \mathcal{V} = \mathcal{L}^* V \mathcal{L}^{*T},$$

$$\mathcal{U}_{(x)} = \mathcal{L}^{*\prime} U \mathcal{L}^{*T}, \quad \mathcal{U}_{(y)} = \mathcal{L}^* U \mathcal{L}^{*\prime T},$$

where we have introduced the matrices containing the point values of the basis functions and of their derivatives at the same Gauss–Legendre points,

$$\mathcal{L}^* \equiv \left\{ \mathcal{L}^*_{h,n} = L^*_n(x_h),\, 1 \le h \le \frac{3}{2}(N+1),\, 0 \le n \le N \right\},$$
$$\mathcal{L}^{*\prime} \equiv \left\{ \mathcal{L}^{*\prime}_{h,n} = L^{*\prime}_n(x_h),\, 1 \le h \le \frac{3}{2}(N+1),\, 0 \le n \le N \right\}.$$

The array $\mathcal{C} = \{\mathcal{C}_{h,k}, 1 \le (h,k) \le \frac{3}{2}(N+1)\}$ of the point values of the nonlinear term $c_N(x,y)$ is obtained from the relation

$$\mathcal{C} = \mathcal{U} \star \mathcal{U}_{(x)} + \mathcal{V} \star \mathcal{U}_{(y)},$$

where $\star$ denotes the element-by-element multiplication of matrices. As a consequence, the pseudospectral approximation of the nonlinear term is obtained by projecting (in the L^2 sense) this term by means of the direct-product Gauss–Legendre quadrature formula with $\frac{3}{2}(N+1) \times \frac{3}{2}(N+1)$ points, to give

$$\int_{-1}^{1}\int_{-1}^{1} L^*_n(x),\, c_N(x,y),\, L^*_m(y)\, dx\, dy \approx \sum_{h=1}^{\frac{3}{2}(N+1)} L^*_n(x_h),\, w_h,\, \mathcal{C}_{h,k},\, w_k,\, L^*_m(y_k) \sum_{k=1}^{\frac{3}{2}(N+1)}.$$

We emphasize that the number of points in the quadrature rule has been selected to avoid aliasing errors, which could produce numerical instabilities at high Reynolds numbers [2].

The sought for matrix $C = \{C_{n,m}\}$ of the L^2 projection of the nonlinear term is finally given by

$$C = \mathcal{L}^{*T} \mathcal{W} \mathcal{C} \mathcal{W} \mathcal{L}^*,$$

where the Gauss–Legendre weights have been framed in the diagonal matrix $\mathcal{W} = \mathrm{diag}\,(w_1, w_2, \ldots, w_{\frac{3}{2}(N+1)})$. The nonlinear term $d_N(x,y) = \boldsymbol{u}_N \cdot \boldsymbol{\nabla} v_N$ for the y component of the momentum equation is evaluated by the same procedure. The expression of the contribution of the nonlinear term to the right-hand side of the momentum equation is

$$\boldsymbol{F}_{nl} = -\nu^{-1} \mathcal{L}^{*T} \mathcal{W} \left[\mathcal{U} \star \boldsymbol{\mathcal{U}}_{(x)} + \mathcal{V} \star \boldsymbol{\mathcal{U}}_{(y)} \right] \mathcal{W} \mathcal{L}^*,$$

where $(\mathcal{U}, \mathcal{V}) = \boldsymbol{\mathcal{U}} = \mathcal{L}^* \boldsymbol{U} \mathcal{L}^{*T}$, $\boldsymbol{\mathcal{U}}_{(x)} = \mathcal{L}^{*\prime} \boldsymbol{U} \mathcal{L}^{*T}$, and $\boldsymbol{\mathcal{U}}_{(y)} = \mathcal{L}^* \boldsymbol{U} \mathcal{L}^{*\prime T}$.

5. NUMERICAL RESULTS

5.1. Convergence Rate

To investigate the convergence properties of the spectral projection, we consider the test problem whose analytical solution is

$$u_x = -(\cos x \sin y) g(t),$$
$$u_y = (\sin x \cos y) g(t),$$
$$p = -\frac{1}{4}[\cos(2x) + \cos(2y)] g^2(t),$$

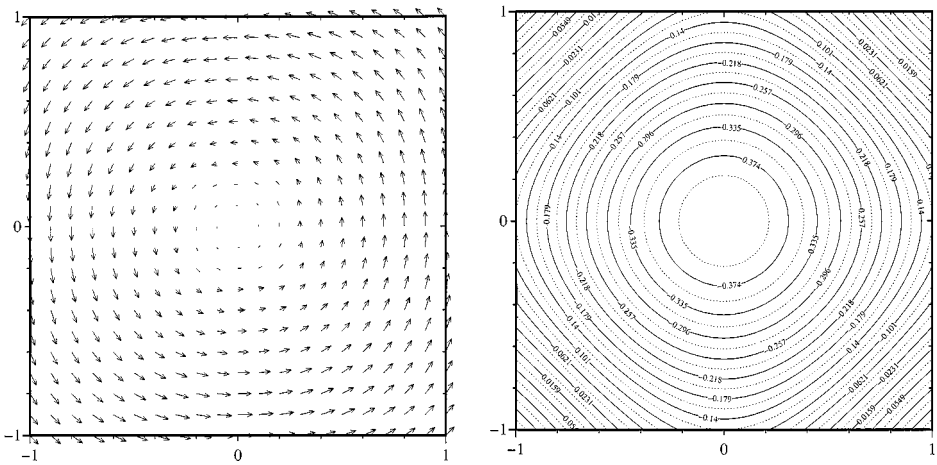

FIG. 2. Velocity (left) and pressure (right) fields for the analytical test case at $t = 1$ for $\mathrm{Re} = 100$.

on the square $\Omega = (-1, 1)^2$. Introducing the velocity in the form $\boldsymbol{u} = \tilde{\boldsymbol{u}}(x, y)g(t)$, the source term corresponding to the momentum equation in the Navier–Stokes system reads $\boldsymbol{f} = \tilde{\boldsymbol{u}}(x, y)[g'(t) + 2g(t)/\mathrm{Re}]$. The exact solution for this test case is shown in Fig. 2, where the velocity and pressure fields are depicted on the left and on the right in the figure.

Two test cases with two different $g(t)$ functions have been performed in order to evaluate the accuracy of the method in both space and time. For the space convergence case, an exponential time dependence, asymptotically approaching a steady state, has been selected, $g(t) = 1 - \exp(-\alpha t)$ with $\alpha = 4$. Spatial convergence results for velocity and pressure at time $t = 200$ are reported in Fig. 3 (left). Here, the $L^2(\Omega)$ and $H^1(\Omega)$ norms of the error,

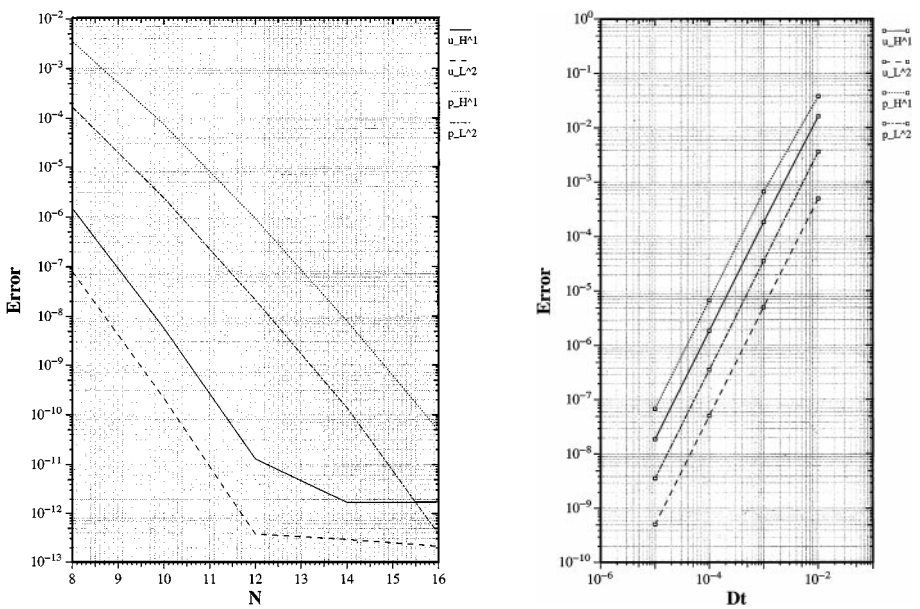

FIG. 3. Space (left) and time (right) convergence rate for the second order BDF projection method.

evaluated numerically by means of the Gaussian quadrature on N points, are displayed. Spectral convergence is obtained for the two variables in both norms. For the time convergence test, a sinusoidal time dependence has been employed, $g(t) = \sin(2t)$. Results are presented in Fig. 3 (right) where the $l^\infty(0, 1; L^2(\Omega))$ and $l^\infty(0, 1; H^1(\Omega))$ norms of the velocity and pressure error are reported: in this case velocity and pressure converge with a second-order rate in both error norms. This result confirms the theoretical estimates provided in [19]. Moreover, the convergence rate displayed by our computations is found not to be corrupted even when the error is measured by norms that are stronger than those considered by the theory.

5.2. Flow Stability in the Singular Driven Cavity

As a second test problem, the simulation of the flow in a square driven cavity is considered. The solution of this problem presents some difficulties because of the singular nature of flow in the regions of the upper corners, where the horizontal wall slides on the stationary vertical walls. At these two points, the boundary value of the horizontal velocity is discontinuous when passing from the fixed vertical walls to the moving horizontal one. As a consequence, the solution of the unregularized problem is characterized by a singular behavior at these points for any Reynolds number. However, the singular component of the solution can be evaluated analytically by an asymptotic expansion described by Gupta *et al.* [22] and can be subtracted from the unknowns to obtain a regular problem, as shown by Botella and Peyret [11]. In the present work this technique has been adopted to avoid the occurrence of spatial oscillations in the spectral solution caused by Gibbs' phenomenon.

The time accuracy of the proposed methods is assessed by computing unsteady solutions for an impulsive start of the wall (note that, in any case, $\boldsymbol{n} \cdot \boldsymbol{b} = 0, t \geq 0$) at Re = 1000. The vorticity field and the streamlines at time $t = 6.25$ computed by the BDF projection method are given in Fig. 4. The secondary eddy developing on the vertical wall shown in Fig. 4 is identical in shape and intensity to that obtained by a spectral biharmonic solver based on the Glowinski–Pironneau method [3]. Moreover, the vorticity field at same time is virtually indistinguishable from the corresponding solution provided by the

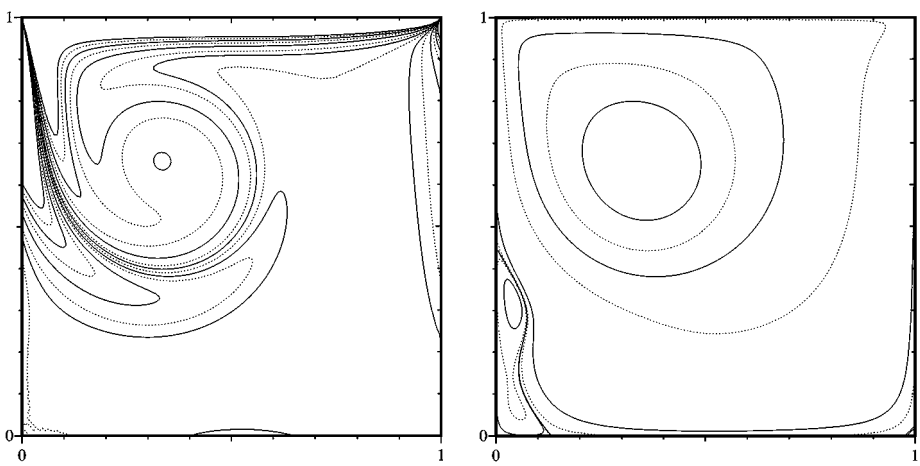

FIG. 4. Vorticity field and streamlines for the impulsively started driven cavity flow for Re = 1000 at $t = 6.25$. Solution computed by the BDF spectral projection method with $N = 96$ and $\tilde{N} = 94$.

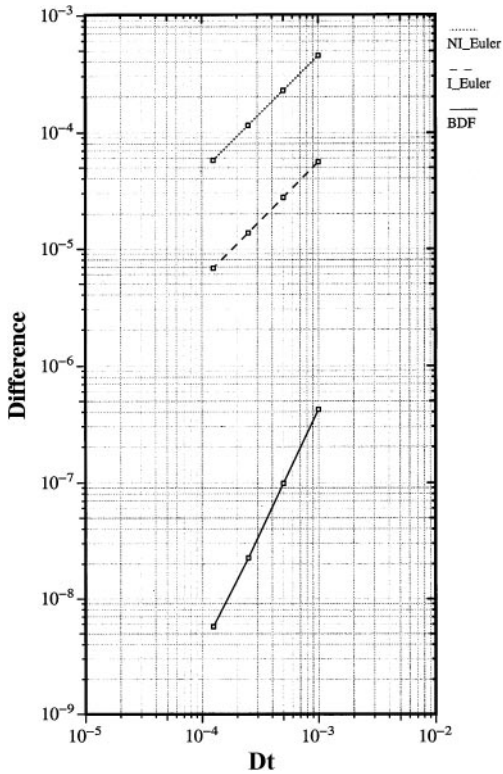

FIG. 5. Differences between the value of the stream function in the center of the cavity at $t = 6.25$ and $\mathrm{Re} = 1000$ for varying Δt. Differences between values computed by different spectral projection methods (a nonincremental scheme, a first-order incremental scheme and the proposed second-order BDF scheme) with the reference values provided by a $\mathcal{O}((\Delta t)^2)$ accurate spectral biharmonic solver with $N = 96$ and $\hat{N} = 94$.

vorticity-stream function solver once the latter is associated with the aforementioned technique of singularity subtraction [5]. In Fig. 5 we compare the point value of the stream function in the center of the cavity computed with the proposed projection methods with the value obtained by the vorticity-stream function solver with a second-order BDF time integration we have implemented. The differences shown in this figure between the results of the BDF projection method and the reference values can be hardly commented.

The performance of the proposed algorithm, run on a Digital 433au workstation with 128 Mbytes of RAM memory, can be evaluated from the data in Table I where the CPU time in seconds per time step is reported. In the same table, the CPU time per time step per mode is also reported from which the efficiency of the method can be appreciated.

TABLE I
Performance of the Proposed Algorithm

N	Cpu time per time step (s)	Cpu time per time step per mode (s)
16	0.00278	1.0859×10^{-5}
32	0.01068	1.0430×10^{-5}
64	0.06376	1.5566×10^{-5}
128	0.38021	2.3206×10^{-5}

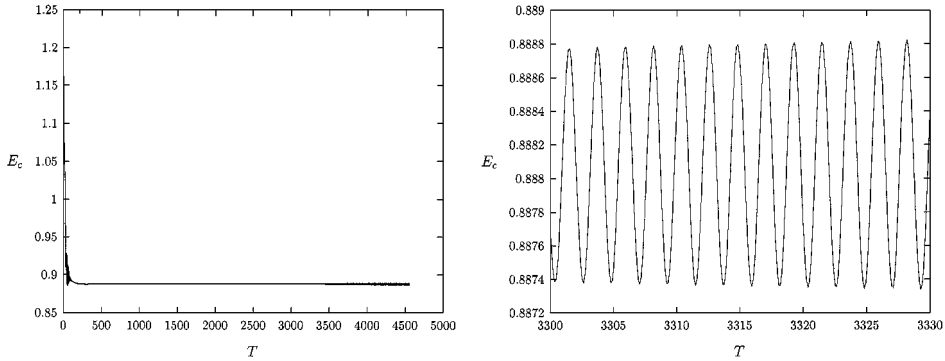

FIG. 6. Total kinetic energy of the cavity flow with Re = 8125: complete time history (left) and asymptotic periodic behavior, $f = 0.450$ (right).

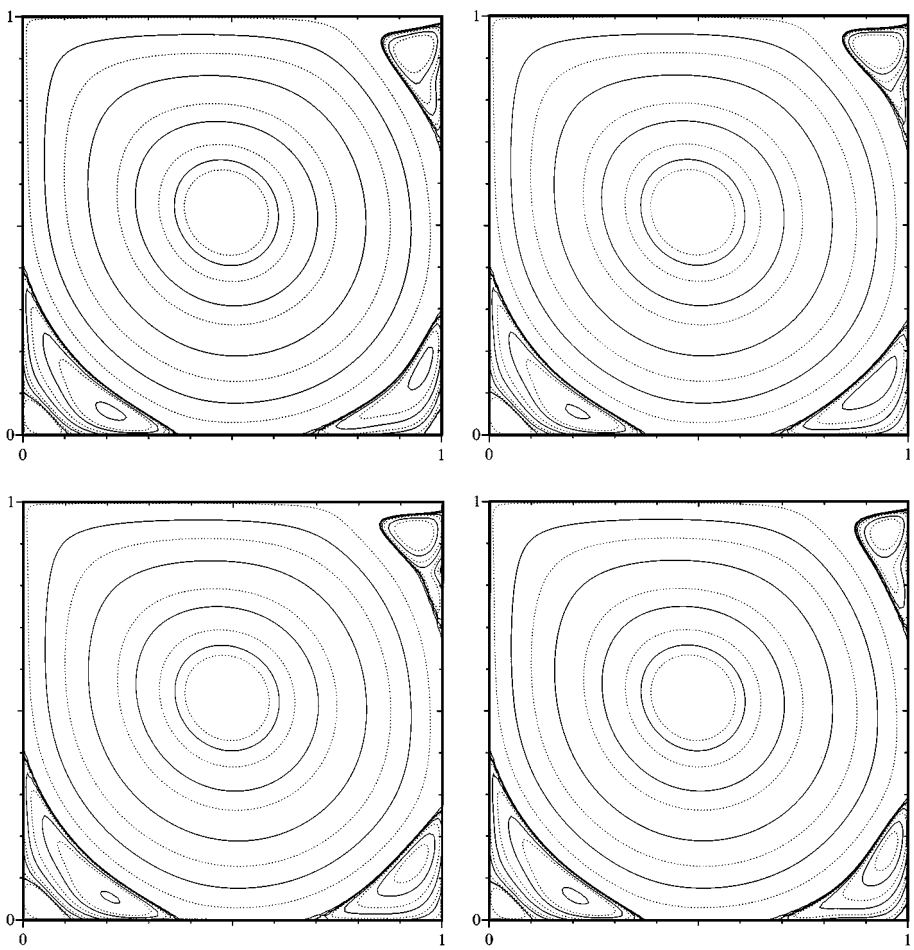

FIG. 7. Streamlines of the periodic solution for Re = 8125 at four times separated by the time interval $T/4 = 1/(4f) = 0.555$.

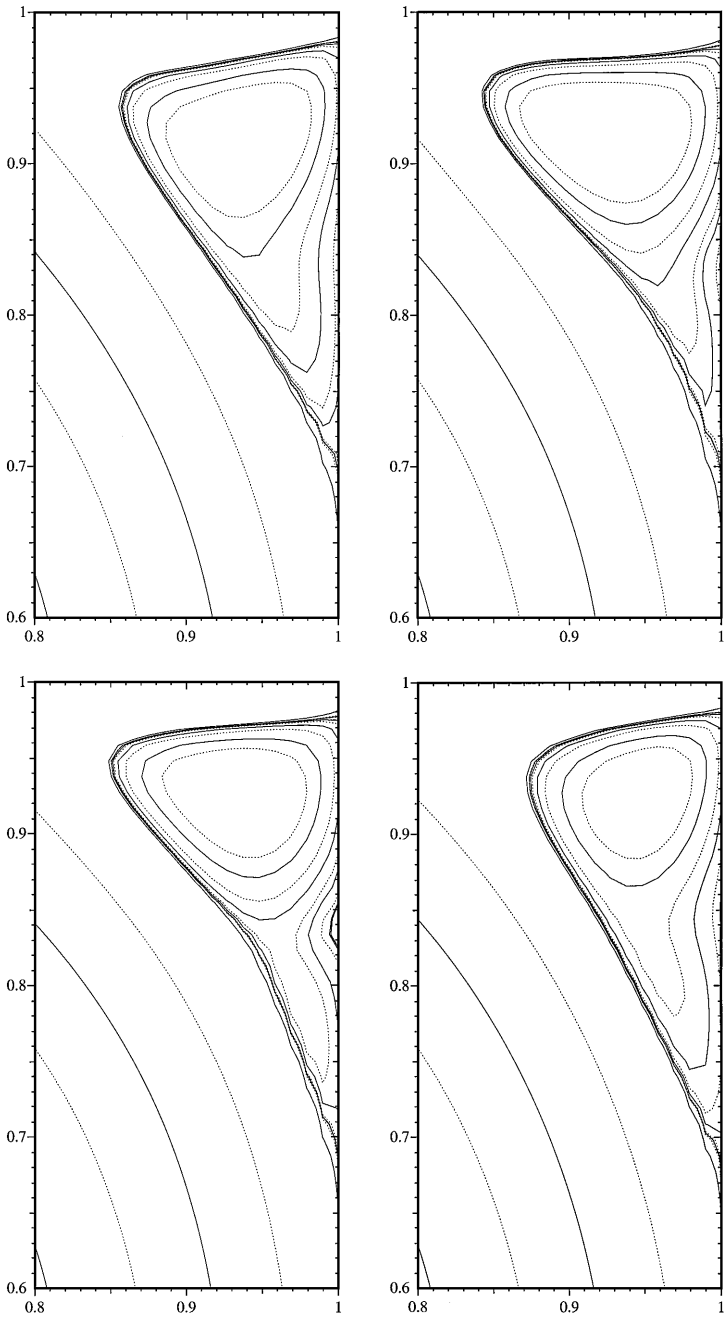

FIG. 8. Top right corner (detail).

By means of the proposed BDF spectral projection scheme, we have investigated the first Hopf bifurcation of the flow in the singular driven cavity problem. The critical Reynolds number for the first transition to a periodic flow has been precisely localized to be in the range $8017.6 < \mathrm{Re}_{\mathrm{crit}} < 8018.8$ [1]. Just to give an idea of the accuracy permitted by the proposed method in simulating unsteady flows, we present here the solution at a Reynolds number $\mathrm{Re} = 8125$ slightly above the bifurcation. For such a value, the asymptotic solution is periodic

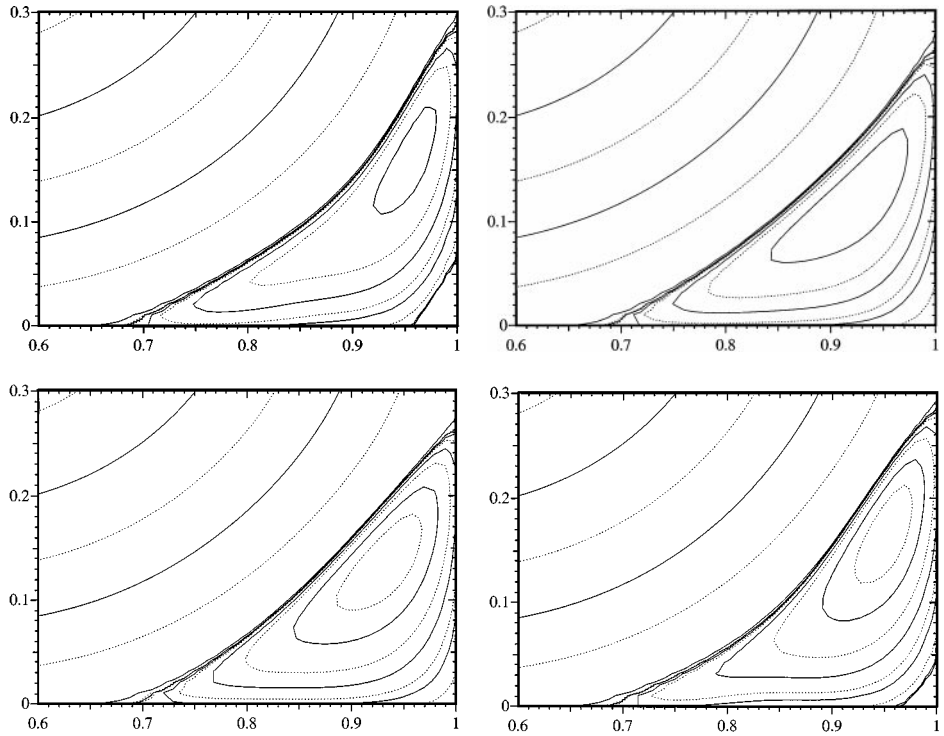

FIG. 9. Bottom right corner (detail).

with a frequency $f = 0.450$. The oscillatory behavior is represented in Fig. 6 by means of the time evolution of the kinetic energy of the regular component of the velocity field integrated over the cavity. The asymptotic state of the flow is presented in Fig. 7 reporting the streamlines at four times separated by the time interval $T/4 = 1/(4f) = 0.555$, which corresponds to a complete cycle. The unsteady character of the flow is more evident in the secondary eddies located in the top- and bottom-right corners, shown in the enlargement given in Figs. 8 and 9, respectively.

6. CONCLUSIONS

In this paper we presented a new Galerkin–Legendre spectral implementation of the second-order incremental scheme proposed and analysed in a discrete abstract functional setting for both finite elements and spectral approximations in [18]–[21]. The convergence properties of the scheme predicted by the theory are confirmed by the numerical tests shown in the paper. Our tests indicate that the incremental projection method has a second-order error, confirming that, also in the spectral case, the time-splitting error of this method is of second order, which is not the case for its nonincremental counterpart.

The proposed spectral projection method adopts two different bases for the spatial approximation of the velocity and pressure fields but does not require the introduction of any grid for the solution of the uncoupled linear subproblems provided by the fractional-step strategy. In other words, in the new algorithm, all the linear terms are treated completely in the coefficients domain, without any transformation in or from the physical space. Quite notably, most of the matrices representing the one-dimensional spatial differential

operators are banded and can be expressed in closed form so that the preprocessing phase of the computation is indeed reduced to a minimal amount. As far as the nonlinear convective terms are concerned, they are taken into account by means of a pseudospectral technique based on Gauss–Legendre quadrature points. A quadrature formula with $\frac{3}{2}N$ points has been selected to preclude aliasing errors. This possibility is offered by the noncollocative nature of the method in which hierarchical polynomial bases are employed as opposed to nodal Lagrangian interpolants.

A great simplification in the proposed approach is allowed by the elimination of the end-of-step velocity with the associated need for solving mass matrix problems to determine such a velocity. As a consequence, the proposed scheme is very easy to implement and turn out to be very efficient, as shown by the tests performed in the paper. We reached a very fast algorithm which allowed us to perform the long, time simulations required to investigate the stability of the driven cavity flow [1] on an entry level workstation. The same algorithm is currently extended straightforwardly to deal with three-dimensional problems, and the same projection scheme has been recently implemented with spectral/p elements [6].

REFERENCES

1. F. Auteri and N. Parolini, First Hopf bifurcation in the singular driven cavity flow, presented at Fourth EUROMECH Fluid Mechanics Conference, Eindhoven, 2000.
2. F. Auteri and N. Parolini, Quadrature of convective term and stability of weak pseudospectral projection methods, submitted for publication.
3. F. Auteri and L. Quartapelle, Galerkin spectral method for the vorticity and stream function equations, *J. Comput. Phys.* **149**, 306 (1999).
4. F. Auteri and L. Quartapelle, Galerkin–Legendre spectral method for the 3D Helmholtz equation, *J. Comput. Phys.* **161**, 454 (2000).
5. F. Auteri, L. Quartapelle, and L. Vigevano, Accurate ω-ψ spectral solution of the singular driven cavity problem, submitted for publication.
6. F. Auteri, F. Saleri, and L. Vigevano, Incompressible Navier–Stokes solutions by a triangular spectral/p element projection method, *Comput. Methods Appl. Mech. Engrg.* **190**, 6927 (2001).
7. I. Babuška, The finite element method with Lagrangian multipliers, *Numer. Math.* **20**, 179 (1973).
8. A. Batoul, H. Khallouf, and G. Labrosse, Une méthode de resolution directe (pseudo-spectrale) du problème de Stokes 2D/3D instationnaire. Application à la cavité entraînée carrée, *Comput. Fluids* **26**, 107 (1997).
9. C. Bernardi and Y. Maday, *Approximations spectrales des problèmes aux limites elliptiques* (Springer-Verlag, Paris, 1992).
10. O. Botella, On the solution of the Navier–Stokes equations using Chebyshev projection schemes with third order accuracy in time, *Comput. Fluids* **26**, 107 (1997).
11. O. Botella and R. Peyret, Benchmark spectral results on the lid-driven cavity flow, *Comput. Fluids* **27**, 421 (1998).
12. F. Brezzi, On the existence uniqueness and approximation of saddle-point problems arising from Lagrangian multipliers, *R.A.I.R.O.* **R.2**, 129 (1974).
13. C. Canuto, M. Y. Hussaini, A. Quarteroni, and T. A. Zang, *Spectral Methods in Fluid Mechanics* (Springer-Verlag, New York, 1988).
14. A. J. Chorin, Numerical solution of the Navier–Stokes equations, *Math. Comp*. **22**, 745 (1968).
15. A. J. Chorin, On the convergence of discrete approximations to the Navier–Stokes equations, *Math. Comp.* **23**, 341 (1969).
16. K. Goda, A multistep technique for the with implicit difference schemes for calculating two- or three-dimensional cavity flows, *J. Comput. Phys.* **30**, 76 (1979).

17. D. Gottlieb and S. A. Orszag, *Numerical Analysis of Spectral Methods: Theory and Applications* (Soc. for Industr. & Appl. Math., Philadelphia, 1977).
18. J.-L. Guermond, Sur l'approximation des équations de Navier–Stokes par une méthode de projection, *C. R. Acad. Sci. Paris, Série I* **319**, 887 (1994).
19. J.-L. Guermond, Un résultat de convergence à l'ordre deux en temps pour l'approximation des équations de Navier-Stokes par une technique de projection, *Modél. Math. Anal. Numér. (M^2AN)* **33**, 169 (1999).
20. J.-L. Guermond and L. Quartapelle, Calculation of incompressible viscous flows by an unconditionally stable projection FEM, *J. Comput. Phys*. **132**, 12 (1997).
21. J.-L. Guermond and L. Quartapelle, On the approximation of the unsteady Navier–Stokes equations by finite element projection methods, *Numer. Math*. **80**, 207 (1998).
22. M. M. Gupta, R. P. Manohar, and B. Noble, Nature of viscous flows near sharp corners, *Comput. Fluids* **9**, 379 (1981).
23. W. Heinrichs, Splitting techniques for the pseudospectral approximation of the unsteady Stokes equations, *SIAM J. Numer. Anal*. **30**, 19 (1993).
24. W. Heinrichs, High-order time splitting for the Stokes equations, *J. Sci. Comput*. **11**, 397 (1996).
25. W. Heinrichs, Splitting techniques for the unsteady Stokes equations, *SIAM J. Numer. Anal*. **35**, 1646 (1998).
26. G. E. Karniadakis, M. Israeli, and S. A. Orszag, High-order splitting methods for incompressible Navier-Stokes equations, *J. Comput. Phys*. **97**, 414 (1991).
27. H. C. Ku, T. D. Taylor, and R. S. Hirsh, Pseudospectral methods for solution of the incompressible Navier–Stokes equations, *Comput. Fluids* **15**, 195 (1987).
28. H. C. Ku, T. D. Taylor, and R. S. Hirsh, A pseudospectral method for solution of the three-dimensional incompressible Navier–Stokes equations. *J. Comput. Phys*. **70**, 439 (1987).
29. O. A. Ladyshenskaya, *The Mathematical Theory of Viscous Incompressible Flow*, 2nd. ed. (Gordon & Breach, New York, 1969).
30. J. M. Lopez and J. Shen, An efficient spectral projection method for the Navier–Stokes equations in cylindrical geometries I. Axisymmetric cases, *J. Comput. Phys*. **139**, 308 (1998).
31. S. A. Orszag and L. C. Kells, Transition to turbulence in plane Poiseuille flow and plane Couette flow, *J. Fluid Mech*. **96**, 159 (1980).
32. L. Quartapelle, *Numerical Solution of the Incompressible Navier–Stokes Equations* (Birkhäuser, Basel, 1993).
33. R. Rannacher, On Chorin's projection method for the incompressible Navier–Stokes equations, in *The Navier–Stokes Equations II. Theory and Numerical Methods*, Lecture Notes in Mathematics (Springer-Verlag, Berlin/New York, 1991), Vol. 1530, pp. 167–183.
34. Jie Shen, Efficient spectral–Galerkin method. I. Direct solvers of second- and fourth-order equations using Legendre polynomials, *SIAM J. Sci. Comput*. **15**, 1489 (1994).
35. Jie Shen, On error estimates of projection methods for the Navier–Stokes equations: Second-order schemes, *Math. Comp*. **65**, 1039 (1996).
36. G. Szegö, *Orthogonal Polynomials* (Am. Math. Soc. New York, 1959).
37. R. Temam, *Navier–Stokes Equations*, Studies in Mathematics and its Applications (North-Holland, Amsterdam, 1977), Vol. 2.
38. R. Temam, Sur l'approximation de la solution des équations de Navier–Stokes par la méthode de pas fractionnaires, *Arch. Rat. Mech. Anal*. **33**, 377 (1969).
39. J. Van Kan, A second order accurate pressure correction scheme for viscous incompressible flow, *SIAM J. Sci. Stat. Comput*. **7**, 870 (1986).
40. T. A. Zang and M. Y. Hussaini, On spectral multigrid methods for the time-dependent Navier–Stokes equations, *Appl. Math. Comput*. **19**, 359 (1986).